

PREPARATION AND CHARACTERIZATION OF $Mg_xCr_yZn_{1-x-y}O$ NANOPARTICLES OBTAINED BY AUTO COMBUSTION TECHNIQUE

Tagreed M. Al-Saadi¹, Radhwan Shopan Al - Afraijy²

^{1,2} Department of Physics, College of Education for Pure Sciences - Ibn Al-Haitham , University of Baghdad, Al-Jadriya (Post Box No. 47078), Baghdad, Iraq, tagreedmm2000@gmail.com

ABSTRACT: In This study pure and (Mg, Cr) doped ZnO-NPs with various doping concentrations were prepared via sol-gel combustion route from a zinc nitrate precursor and citric acid. The effect of (Mg and Cr) doping on the crystal structure and electrical properties of the ZnO-NPs were demonstrated in this paper. The synthesized un-doped ZnO and ($Mg_xCr_yZn_{1-x-y}O$) were characterized using X-ray diffraction analysis (XRD), scanning electron microscopy (SEM), energy dispersive spectroscopy (EDX) and (LCR meter). The (XRD) patterns indicate that all prepared nanostructures exhibited a hexagonal (wurtzite) structure. The average particle size of ZnO-NPs was calculated using the Debye-Scherrer formula. The resulting powder was found to have a grain size in the nanoscale, lying between (22-33) nm. Frequency dependent dielectric constant and dielectric loss for the pure and doped ZnO nanoparticles were carried out. The variations in ac conductivity dependent frequency and the temperature had also been studied at (room temperature, 50, 100 and 150 °C).

Keywords: doped ZnO-NPs; auto combustion method; XRD; dielectric properties; A.C Electrical conductivity.

1. INTRODUCTION

In the recent years, the semiconductor nanoparticles have much noticeable attention due to their perceptive mechanical, optical and electrical properties, compared with their equivalents in the bulk scale [1, 2]. Amongst them, zinc oxide (ZnO) nanostructures, essentially is an n-type semiconductor, is a gorgeous multifunctional material has a wide implementation in the field of sensors, varistors, solar cells, gas sensors, displays and UV light-emitting devices [3,4]. As a direct wide band gap semiconductor about (3.37) eV, with a large exciton binding energy of (60 meV), ZnO is representing a great attraction for electronic and optoelectronic devices. For instance, a device that made by a larger band gap material might have a lower noise generation, high breakdown voltage, and can run with high power operation at higher temperatures [5, 6]. ZnO nano-sized can be prepared by several techniques, such as hydrothermal, physical vapour deposition, micro-emulsion method [7], co-precipitation [8] and a sol-gel method [9]. Among these techniques, the sol-gel method is appropriate for synthesizing ZnO nanoparticles due to its versatility, simplicity, and low cost. Comparing with other methods, sol-gel technique exhibits advantages in the production of nanoparticles such as relatively low temperatures and short reaction time [10, 11]. Therefore, the appropriate route for preparing doped ZnO Nanopowder with less synthesis time, narrow size range, less operating cost and better features is a challenge for scientists [12]. Meantime, doping with selective elements [13, 14] (R. Viswanatha, *et al*, Mg-doped ZnO, 2012) & (Vishwanath Dattu Mote, *et al*, Cr doped ZnO, 2012) exhibit an effective method to control and enhance the optical and electrical properties of ZnO nanostructures, which is considered as crucial for its practical application. [13]. Hence, in the present study, a simple and cost-effective sol-gel combustion method was used to prepare pure and $Mg_xCr_yZn_{1-x-y}O$ doped ZnO nanoparticles, by utilizing nitrate of Zinc as a precursor and citric acid as a combustion agent. Structural and electrical characteristics of synthesized nanomaterial were investigated by means of XRD, SEM, EDX and LCR meter. The obtained results were matching well with literature.

2. EXPERIMENTAL DETAILS

In the synthesis processes, the Chemicals were used are Zinc nitrate $Zn(NO_3)_2 \cdot 6H_2O$, Magnesium nitrate $Mg(NO_3)_2 \cdot 6H_2O$, Chromium nitrate $Cr(NO_3)_3 \cdot 9H_2O$, Citric Acid ($C_6H_8O_4$), Ammonia solution (NH_3), and Distilled water.

To prepare (40 g) of pure and doped ZnO-NPs, (60 mL) of distilled pure water was mixed with the nitrates of (Zn, Mg and Cr) and (14.1222 g) of citric acid, note that the citric acid ratio was constant for each sample. The solutions mixed in a heat-resistant beaker by a magnetic stirrer for (40 min) at room temperature to ensure the full homogeneity of the solution. After placing the solution on a magnetic stirrer, the temperature has been gradually raising and stabilized at 85°C. After a duration of time, gases began to evaporate, after this, the interaction left for a while with continuation moving the solution until the viscous gel form consists. After about (50 min), gel began to ignition to form a dry gel (xerogel), then heat element has been turned off, then the material left to be cool, then collected, then milled well by mortar of ceramic to ensure powder homogeneous and gets rid of the conglomerates that have taken place during the annealing process. Finally, a xerogel was calcined for (2 h) at 600 °C to obtain the nano-scale powder.

3. RESULTS AND DISSECTION

3.1. X-Ray Diffraction Analysis

The phase purity and crystal structure of prepared pure ZnO and different composition of (Mg, Cr) doped ZnO nanoparticles, annealed at 600°C were characterized using X-ray diffraction. A typical XRD spectra shown in figure (1), of pure ZnO and $Mg_xCr_yZn_{1-x-y}O$ for constant value of (x) as Mg content where (x =0.05 Mg, y= 0, 0.05, 0.10, 0.15 and 0.20 Cr) nano-particles. The XRD patterns have revealed that the diffraction peaks of pure and (Mg, Cr) doped ZnO nanoparticles, can be indexed to a hexagonal wurtzite structure. From the diffraction patterns of all prepared samples, four clear peaks of zinc oxide were observed, within the angular range of the X-ray diffraction (20° -80°), ascribed to the crystalline surfaces (101), (100), (002) and (110). The prevalent orientation was at the surface (101), which is matched well with the standard (JCPDS) file for ZnO, (JCPDS36-1451, (a= 0.3279 nm), (c= 0.5204 nm)),

with a space group of (P63mc). It is suggested that the (wurtzite) structure is unchanged, with all different concentrations of doping. For doped samples, a slightly shifted was observed in the peaks of the diffraction pattern as compared to un-doped ZnO sample. As the concentrations doping increases, this shows a small variation in the lattice constants occurs. The unit cell volume was also noted to decrease with increasing Cr content; this indicates that (Cr) ions go to Zn site in ZnO lattice structure. The nanoparticles exhibited changes in relative intensities and crystallite size with changing the doping concentrations. The intensity of ZnO peaks, especially at the clear peak (101), decreases with increasing chromium amount, Fig. (1), this indicating that phase separation has taken place in and such structural degeneration in the ZnO lattice may be imputed to the introduction of the foreign impurity. The crystallinity dependent properties of crystals are attributed to its crystallite size. Larger crystallites develop sharper peaks on the XRD pattern for each crystal plane [15].

3.2. Calculation of Grains Size

The peak width at half maximum was used to evaluate crystallite size (D), for the peaks that have the highest intensity, by using the Scherer formula [16]:

$$D = \frac{k\lambda}{\beta \cos \theta} \quad (1)$$

Where: (D) the grain size, λ : the wavelength of used x-ray (0.15406 nm) for Cu target $K\alpha$ radiation: represents ($FWHM$) the full width at half maximum in radians, θ is Bragg's angle and k : a constant related to the shape of the particles with value approximately equal to (0.89) [17]. Using this formula, the average crystallite size of prepared nanoparticles was found to be equal to (22-33) nm. The values of grains size were found to be decreased with increasing Cr concentration, Table (1). This could be imputed to the ionic radii of Zn, Mg and Cr ions. This is mainly because of subsequent growth rate and the nucleation with increasing Cr due to the difference between the ionic radii of the above-mentioned elements [8]. Respective values of crystallite size (D) represented in Table (1). The relatively high value of crystallite size confirms the well crystalline nature of the material.

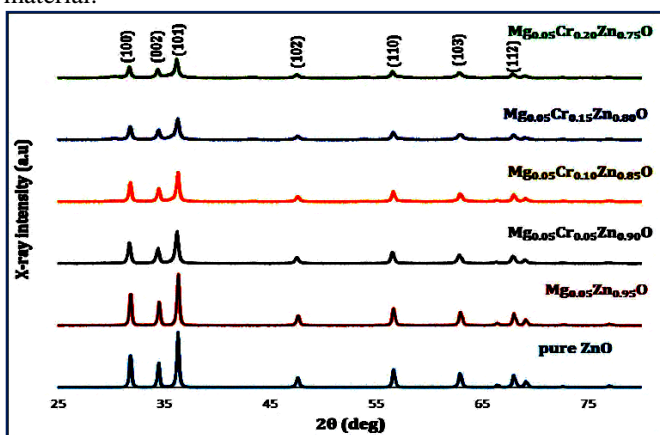


Figure 1: The XRD spectra of undoped and (Mg, Cr) doped ZnO nanoparticles

3.3. Calculation of Specific Surface Area

The Specific surface area is described as a property of materials. It has a particular importance in the case of

reactions on surfaces, adsorption, and heterogeneous catalysis. The Specific area (SSA) can be obtained using Sauter's formula [18]:

$$SS.A = \frac{6 \times 10^3}{D_p \cdot \rho} \quad (2)$$

Where: SS.A is the specific area ($m^2 \cdot g^{-1}$), D_p is the grains size and ρ is the density of the synthesized material. It was noted that the surface area (SS.A) of prepared nanoparticles decreased with increasing particle size. Un-doped ZnO and (5% Mg) prepared sample exhibited lower (SSA) than the samples doped with Mg and Cr, as well as increasing with increasing Cr concentration. Accordingly, it was found to be increased by increasing Cr content, the values of (SS.A) are shown in the table (1).

Table 1: grain size and specific area

| Samples concentrations | grain size (nm) | SS.A ($m^2 \cdot g^{-1}$) | lattice parameters (Å) | | Cell Vol. (Å) ³ |
|--|-----------------|-----------------------------|------------------------|-------|----------------------------|
| | | | a = b | c | |
| Pure ZnO | 33.51 | 31.45 | 3.247 | 5.201 | 54.82 |
| Mg _{0.05} Zn _{0.95} O | 33.15 | 31.8 | 3.248 | 5.197 | 54.8 |
| Mg _{0.05} Cr _{0.05} Zn _{0.90} O | 25.27 | 41.62 | 3.244 | 5.193 | 54.6 |
| Mg _{0.05} Cr _{0.10} Zn _{0.85} O | 28.7 | 36.71 | 3.247 | 5.197 | 54.8 |
| Mg _{0.05} Cr _{0.15} Zn _{0.80} O | 22.46 | 46.87 | 3.246 | 5.194 | 54.74 |
| Mg _{0.05} Cr _{0.20} Zn _{0.75} O | 25.2 | 41.79 | 3.247 | 5.198 | 54.8 |

3.4. Morphological and Elemental Analysis

The surface morphology and elemental analysis of the prepared nanoparticles (Mg_{0.05}Cr_{0.05}Zn_{0.90}O), was investigated by the electronic microscope (SEM), fitted with an energy dispersive X-ray spectroscopy (EDX) device.

The image of SEM showed nanoparticles with average size of (30.399) nm. In SEM, the particle size was calculated by taking the remarkable grain boundaries. While in XRD, the measurements are taken from a crystalline area that diffracts the X-ray waves [19]. Thus, the particle size measurement of (Mg_{0.05}Cr_{0.05}Zn_{0.90}O) using XRD was found to be smaller than that with SEM measurement.

EDX relatively considered a rapid and nondestructive approach for surface analysis. Composition and purity of the sample were studied using EDX. It is often used to survey surface analytical problems and elemental analysis. The higher peak in a spectrum, the more concentrated element is in the sample. The observed peaks reveal the presence of Zn, Mg, Cr and O, that is confirming the formation of the analysed sample. EDX spectra for (Mg, Cr) doped ZnO sample proved the existence of Zn, oxygen, magnesium and chromium. The peak values at (1.012) and (8.637) keV, confirm the presence of zinc, the peak at (0.525) keV exhibits the presence of oxygen, the peak at (0.572 and 5.415) keV shows the presence of chromium and the peak at (1.254) keV reveals the presence of magnesium in the EDX spectra, fig. (2).

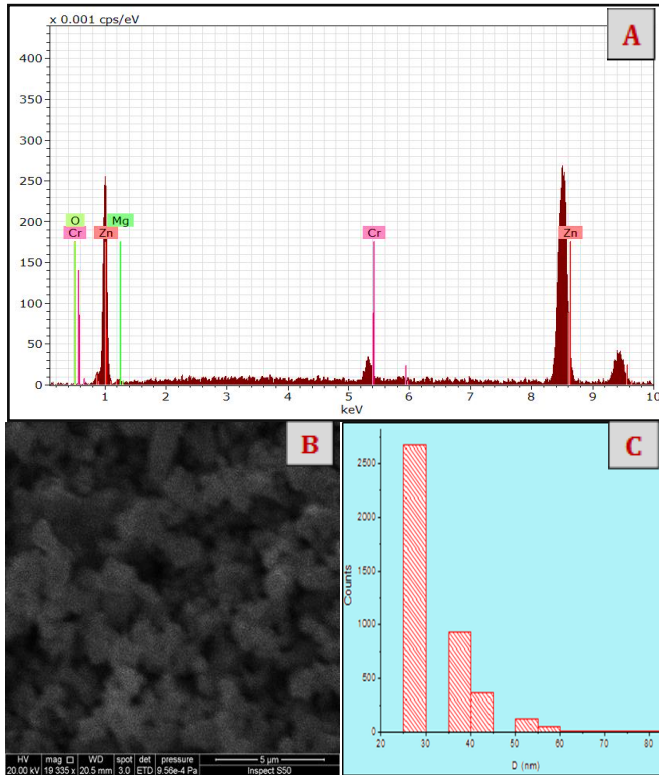


Figure 2: A. EDX spectra for the sample (5% Mg & 5% Cr) doped ZnO; B. SEM image; and C. average crystallite size calculated from SEM image.

3.5.Electrical Studies

One of the most important features of semiconductors is that it has a negative thermal coefficient, this leads to increased electrical conductivity of the semiconductor with increasing temperature due to the collapse of the bonds and the transfer of electrons from the valence band to the conduction band, these features have made semiconductor very useful in many electronic applications [20].

3.5.1 Frequency dependent Dielectric constant (ϵ_r') and dielectric loss factor (ϵ_r'')

The dielectric parameter as a function of the frequency can be characterized by a complex permittivity [21]:

$$\epsilon(\omega) = \epsilon_r'(\omega) - \epsilon_r''(\omega) \tag{3}$$

Here the real part (ϵ_r') and imaginary part (ϵ_r''), which represent the combinations of the stored energy and energy loss, respectively, for each cycle of the electric field, and (ω) is an angular frequency ($\omega = 2\pi f$), f is applied frequency.

The dielectric constant (ϵ_r'), it represents the relative dielectric constant or real permittivity which is ordinarily called dielectric constant of exam material. Dielectric constant (ϵ_r') is computed from the measurements of the capacitance value. Using the following equation, the dielectric constant can be obtained [22]:

$$\epsilon_r' = \frac{t * C_p}{A * \epsilon_0} = \frac{t * C_p}{\pi \left(\frac{d}{2}\right)^2 * \epsilon_0} \tag{4}$$

Where, (t): is the thickness of the pellet, C_p : parallel capacitance obtained from data of measurement, (ϵ_0): the vacuum permittivity equal to = 8.854×10^{-14} (F/cm), A : area of the electrode and d : Diameter of guard electrodes.

Generally, ZnO is described as a polar molecule this fact is well-known. It has a permanent dipole moment and quickly responds to the applied electric field. It is clear from the fig. (3), It was observed a similar behaviour of all models, where, with increasing the frequency of the applied electric field, the dielectric constant is clearly reduced. In addition, it was also noticed that the dielectric constant values approximately remain constant at high frequencies. At low frequencies, pure ZnO have the large values of dielectric constant, this is due to the domination of species of vacancies such as oxygen and defects of grain boundary etc. Whereas, the decreasing of dielectric constant with applied frequency is normal, in respect to the reality that any species participating to polarizability is bound to exhibit lagging behind the applied electric field at greater frequencies. Through the noticed the higher value of dielectric constant of doped ZnO, we can deduce that the electron exchange between Zn^{2+} , Mg^{2+} and Cr^{3+} ions at lower frequencies, is predominant. At higher frequencies, the dielectric constant tends to reach almost a constant value due to the fact, which beyond certain frequency the electron exchange between Zn^{2+} , Mg^{2+} and Cr^{3+} cannot go after the applied a.c field [23, 5].

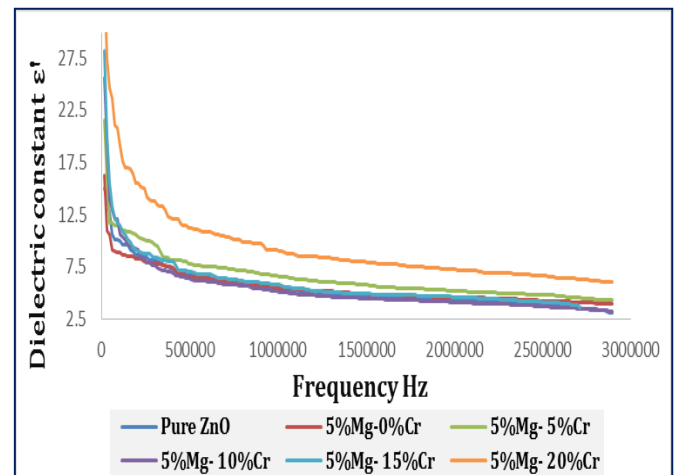


Fig.3. Dielectric constant as a function of frequency, which shows a decrease in dielectric constant with increased frequency.

While, dielectric loss(ϵ_r'') or the imaginary permittivity is evaluated from the value of the dissipation factor (D), where [24]:

$$\tan \delta = D \tag{5}$$

$$D = \frac{\epsilon_r''}{\epsilon_r'} \tag{6}$$

$$\epsilon_r'' = D * \epsilon_r' \tag{7}$$

The energy losses are determined by (ϵ_r''). In an engineering implementation of dielectrics in capacitors, minimal ϵ_r'' is permanently favored for a given (ϵ_r'). The relative magnitude

of ϵ_r'' with respect to ϵ_r' is defined as $(\tan \delta)$, which called as dissipation factor (D) or the loss factor.

In dielectric materials, the losses are commonly occurred due to the current absorption. The molecules orientation along the direction of an electric field in the polar dielectrics demands a part of the electric energy to cope forces of the interior friction. The other part of the electric energy is specified for rotation of dipolar molecules, and other types of molecular transmit from a site to another, which also encompass an energy loss [25].

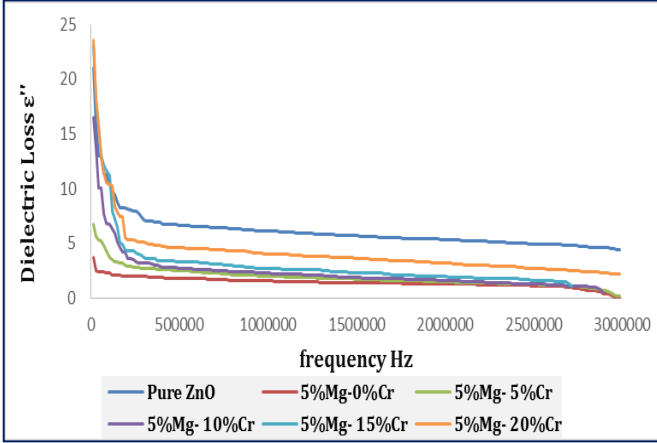


Fig. 4. The variation in dielectric loss versus frequency.

Fig. (4) Illustrates the variation of dielectric loss values with frequency, a similar behaviour was noted for all samples. Where the highest value of dielectric loss factor is at low frequencies and shows a remarkable decrease by increasing the frequency of the applied electric field. This decreasing is because of the space charge polarization. This exotic attitude, as long as, the very low loss factor in compared to the parent ZnO turn out the synthesized Nano samples appropriate for applications the require a high-frequency device [26].

3.5.2 A.C conductivity dependent frequency and temperature

Electrical conductivity grants a considerable information about conduction mechanism of the dielectric materials. The electric conductivity of doped dielectric materials depends on various parameters, like doping mechanism, preparation technique, temperature and sintering conditions and time [27].

Utilizing equation (8), we can obtain the A.C conductivity [28]:

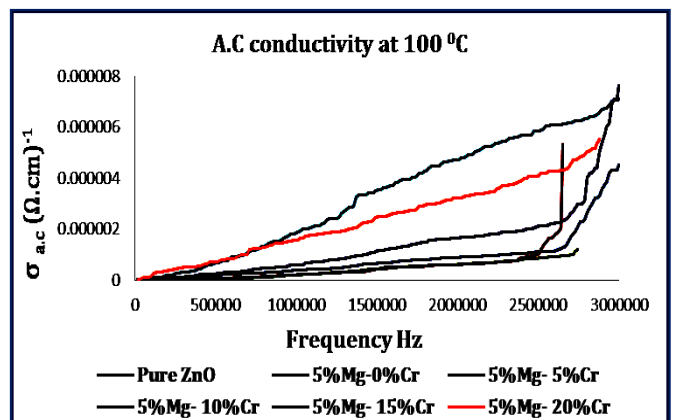
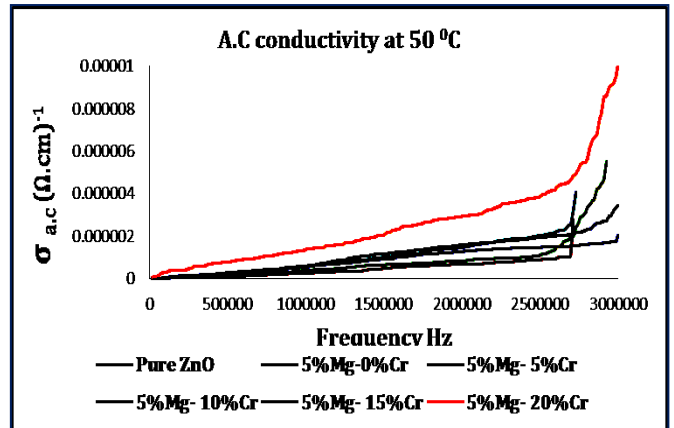
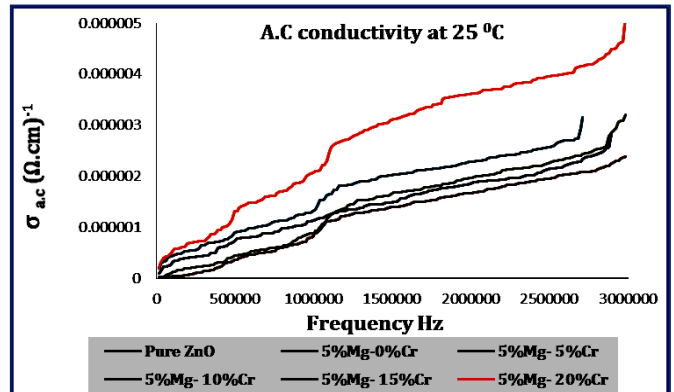
$$\sigma_{ac} = 2\pi f \epsilon_o \epsilon_r' \tan \delta \tag{8}$$

Where, σ_{ac} : Alternative electrical conductivity measured by $(\Omega.cm)^{-1}$, (f) the measuring frequency of the a.c field (Hz), and the dissipation factor $(\tan \delta)$ which characterize the difference in phase between voltage and current with respect to an applied ac field.

The variation of A.C conductivity (σ_{ac}) with the frequency at different temperatures is illustrated by Fig. (5) and Table (2). For all samples, the obtained results showed that the a.c conductivity increases with the increase of the electric field frequency.

Table (2) illustrated the variation of A.C conductivity (σ_{ac}) with the frequency at 100 kHz and different temperatures.

| Temps. | A.C conductivity $(\Omega.cm)^{-1}$ at (2MHz) | | | | | |
|--------|--|-----------------|----------------|-----------------|-----------------|---------------|
| | Undoped ZnO | 5 %Mg 0 %Cr | 5 %Mg 5 %Cr | 5 %Mg 10 %Cr | 5 %Mg 15 %Cr | 5 %Mg 20 %Cr |
| 25 °C | $6*10^{-12}$ | $1.7*10_6^{-7}$ | $1.97*10^{-7}$ | $1.9*10_6^{-6}$ | $2.3*10_6^{-6}$ | $3.6*10^{-6}$ |
| 50 °C | $1.3*10^{-6}$ | $6.9*10_7^{-7}$ | $8.6*10^{-7}$ | $1.6*10_6^{-6}$ | $1.5*10_6^{-6}$ | $2.9*10^{-6}$ |
| 100 °C | $9*10^{-7}$ | $6.2*10_7^{-7}$ | $6.3*10^{-7}$ | $1.7*10_6^{-6}$ | $4.7*10_6^{-6}$ | $3.2*10^{-6}$ |
| 150 °C | $6*10^{-6}$ | $5.6*10_7^{-7}$ | $5.1*10^{-7}$ | $2.4*10_6^{-6}$ | $3.6*10_6^{-6}$ | $4*10^{-6}$ |



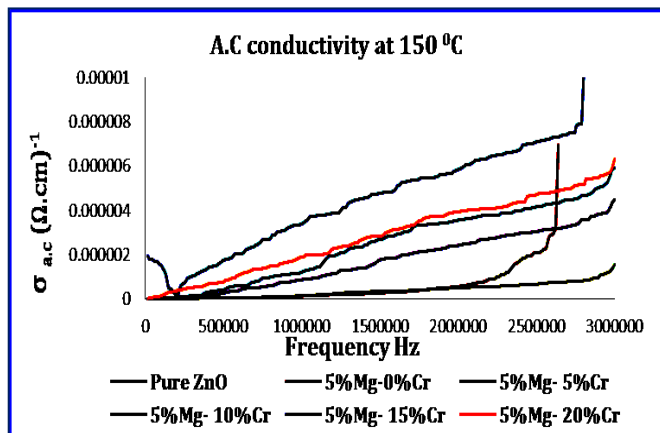


Figure.5: Variation of A.C conductivity with applied frequency at 25, 50, 100 and 150 °C for prepared NPs.

The linear increase in a.c conductivity as the frequency increased, can be interpreted as the increase in frequency has improved the electrons hopping between the charges carriers and thus increasing the electric conductivity of the nanoparticles. As concerning temperature effect on a.c conductivity, it was found that the A.C conductivity was increased as the temperature increased, thus confirming the semiconducting behaviour of the synthesized material. The increasing of a.c electrical conductivity as increasing temperature and frequency may be attributed to the increase in the drift mobility of the electrons and holes by the hopping conduction. Moreover, the increasing in a.c conductivity can be explained as that the increasing in temperature can thermally activate the charge carriers, which in turn increases the charge exchange interactions [27, 29].

4. CONCLUSION

In summary, we have successfully synthesized un-doped $Mg_xCr_yZn_{1-x-y}O$ doped ZnO with an average crystallite size of (22-33) nm by sol-gel auto combustion technique, and the experimental investigations on structural and dielectric properties were carried out at room temperature. The XRD results confirmed a single-phase polycrystalline formation of prepared Nanopowders. The dielectric constant and dielectric loss factor were found to decrease with increasing frequency of the applied electric field. The electrical conductivity behaviour also shows dependent on the frequency, temperature and composition, where it was found to increase with increasing frequency and temperature.

REFERENCES

- [1] C. Chena, B. Yua, P. Liub, J.F. Liua and L. Wanga, "Investigation of nano-sized ZnO particles fabricated by various synthesis routes", *Ceramic Processing Research*. Vol. 12, No. 4, pp. 420-425 (2011).
- [2] M. W. Muayad, "Synthesis and Characteristics Study of ZnO/Porous Si Hetrojunction", M.Sc. thesis, Department of Applied Sciences, University of Technology, (2013).
- [3] L. Upadhyaya, J. Singh, V. Agarwal, A.C. Pandey, S. P. Verma, P. Das and R. P. Tewari, "In situ grafted nanostructured ZnO/carboxymethyl cellulose nanocomposites for efficient delivery of curcumin to cancer", *J Polym Res*, Vol. 21, p.550, (2014).
- [4] S. B. Rana, P. Singha, A. K. Sharmab, A. W. Carbonaric, R. Dograd, "Synthesis and characterization of pure and doped ZnO nanoparticles", *Journal of optoelectronics and advanced materials* Vol. 12, No. 2, p. 257 – 261, Feb (2010).
- [5] M. L. Dinesha, G. D. Prasanna, C. S. Naveen and H. S. Jayanna, "Structural and dielectric properties of Fe doped ZnO nanoparticles", *Indian J Phys*, 85.35.-p; 73.22.-f; 85.50.-n, (2012).
- [6] J. Zhang, D. Gao, G. Yang, J. Zhang, Z. Shi, Z. Zhang, Z. Zhu and D. Xue, "Synthesis and magnetic properties of Zr doped ZnO Nanoparticles", *Nanoscale Research Letters*, Vol.6, p.587, (2011).
- [7] T.V.Kolekar, H.M.Yadav, S.S.Bandgar, A.C.Raskar, S.G.Rawal and G.M.Mishra, "Synthesis by Sol-gel Method and Characterization of Zno Nanoparticles", *Indian Streams Research Journal* Vol -1, ISSUE -1, Feb (2011).
- [8] V. D. Mote, V. R. Huse, B. N. Dole, "Synthesis and Characterization of Cr Doped ZnO Nanocrystals", *World Journal of Condensed Matter Physics*, vol.2, pp. 208-211, (2012).
- [9] J. Ungula, "Growth and characterization of ZnO nanoparticles by sol-gel process", M.Sc. thesis, Department of Physics, University of the Free State (QwaQwa campus), South Africa, (2015).
- [10] S. Xavier, S. Thankachan, B. P. Jacob, E.M. Mohammed, "Effect of Sintering Temperature on the Structural and Magnetic Properties of Cobalt Ferrite Nanoparticles", *Nanosystems: Physics, Chemistry, Mathematics*, Vol. 4, No. (3), P. 430–437, (2013).
- [11] S. Jurablu, M. Farahmandjou, and T. P. Firoozabadi, "Sol-Gel Synthesis of Zinc Oxide (ZnO) Nanoparticles: Study of Structural and Optical Properties", *Journal of Sciences*, Islamic Republic of Iran, Vol. 26(3): pp.281 – 285, (2015)
- [12] S. F. Shayesteh and A. A. Dizgah, "Effect of doping and annealing on the physical properties of ZnO: Mg nanoparticles", *PRAMANA — journal of physics*, Vol. 81, No. 2, pp. 319–330, (2013).
- [13] R. Viswanatha, Y. Arthoba Nayaka, C. C. Vidyasagar and T. G. Venkatesh, "Structural and optical properties of Mg doped ZnO nanoparticles", *Journal of Chemical and Pharmaceutical Research*, Vol. 4(4): pp.1983-1989, (2012).
- [14] Mote, V.D., Huse, V.R. and Dole, B.N., "Synthesis and characterization of Cr doped ZnO nanocrystals". *World Journal of Condensed Matter Physics*, 2(04), p.208, (2012).
- [15] M. M. Abdullah, F. M. Rajab, and S. M. Al-Abbas, "Structural and optical characterization of Cr2O3 nanostructures: Evaluation of its dielectric properties", *AIP Advances* 4, 027121 (2014).
- [16] Samara J. Mohammad, Fadhil Abd Rasin , (2017), "Fabricated Fe-Mn Nanowire as a Binary Oxide by Hydrothermal treatment", *B. Sci. Int. (Lahore)*, 29(6),1351-1354.

- [17] B. Nandana and M. C. Bhatnagarb, "Effect of sintering treatment on structural and magnetic properties of $\text{Ni}_{0.5}\text{Co}_{0.5}\text{Fe}_2\text{O}_4$ Ferrites", AIP Conference Proceedings, 1728, 020506; doi: 10.1063/1.4946557, (2016).
- [18] B. Nath and T. F. Barbhuiya, "Studies on the density and surface area of nanoparticles from *Camellia sinensis*, A natural source", Journal of Chemical and Pharmaceutical Research, Vol. 6(11), PP. 608-610, (2014).
- [19] G. Varughese, P. W. Jithin and K.T. Usha, "Determination of Optical Band Gap Energy of Wurtzite ZnO: Ce Nanocrystallites", Physical Science International Journal, Vol. 5(2): PP. 146-154, (2015).
- [20] A. K. Hashim, S. M. Hadawi and O. M. Yaaser, "New types liquid crystal semiconductor", National Journal of Chemistry, 2006, Vol. 24, PP. 475-487, (2006).
- [21] I. Latif, E. E. AL-Abodi, D. H. Badri and J. Al Khafagi, "Preparation, Characterization and Electrical Study of (Carboxymethylated Polyvinyl Alcohol/ZnO) Nanocomposites", American Journal of Polymer Science, Vol. 2(6): pp. 135-140, (2012).
- [22] K. Omar, M. D. Johan Ooi and M. M. Hassin, "Investigation on Dielectric Constant of Zinc Oxide", Modern Applied Science, Vol.3, No.2, pp.110-116, (2009).
- [23] T. Iqbal, S. Ghazal, S. Atiq, N. R. Khalid, A. Majid, S. Afsheen, and N.A. Niaz, "Influence of Manganese on Structural, Dielectric and Magnetic Properties of ZnO Nanoparticles", Digest Journal of Nanomaterials and Biostructures, Vol. 11, No. 3, p. 899 – 908, (2016).
- [24] Li Li, "Dielectric properties of aged polymers and nanocomposites", Ph.D. thesis, Iowa State University Ames, Iowa, (2011).
- [25] S. Suresh, "Synthesis, structural and dielectric properties of zinc sulfide nanoparticles", International Journal of Physical Sciences, Vol. 8(21), pp. 1121-1127, (2013).
- [26] N. K. Divya, P. U. Aparna and P. P. Pradyumnan, "Dielectric Properties of Er^{3+} Doped ZnO Nanocrystals", Advances in Materials Physics and Chemistry, Vol.5, pp. 287-294, (2015).
- [27] P. Donta, V. K. Katrapally and V. R. Pendyala, "Dielectric Response of $\text{Ni}_x\text{Zn}_{1-x}\text{AlFeO}_4$ Nanoferrites", NanoWorld J, Vol. 2(2), PP. 27-34, (2016).
- [28] T. Das, B.K. Das, K. Parashar and S.K.S. Parashar, "Temperature and Frequency Dependence Electrical Properties of $\text{Zn}_{1-x}\text{Ca}_x\text{O}$ Nanoceramic", ACTA PHYSICA POLONICA A, Vol. 130, No. 6, pp. 1358-1362, (2016).
- [29] A. M. Badr, H. A. Elshaikh and I. M. Ashraf, "Impacts of Temperature and Frequency on the Dielectric Properties for Insight into the Nature of the Charge Transports in the Tl_2S Layered Single Crystals", Journal of Modern Physics, Vol. 2, pp. 12-25, (2011).